Decay processes and radiative cooling of small anionic copper clusters

Christian Breitenfeldt,[1,2] Klaus Blaum,[1] Michael W. Froese,[1] Sebastian George,[1] Gregorio Guzmán-Ramírez,[3] Michael Lange,[1] Sebastian Menk,[1] Lutz Schweikhard,[2] and Andreas Wolf[1]

[1]*Max-Planck-Institut für Kernphysik, D-69029 Heidelberg, Germany*

[2]*Institut für Physik, Ernst-Moritz-Arndt-Universität, D-17487 Greifswald, Germany*

[3]*Departamento de Ingenierías, Centro Universitario de Tonalá, Universidad de Guadalajara, Jal. 48525, Mexico*

(Received 27 June 2016; revised manuscript received 28 July 2016; published 7 September 2016)

The decay of copper clusters Cu_n^- with size $n = 4-7$, produced in a metal ion sputter source, was studied in an electrostatic ion-beam trap. The neutral products after electron emission and fragmentation were monitored for ion storage times of up to a second. The observations indicated the presence of radiative cooling. The energy distributions of the remaining clusters were probed by laser irradiation up to several further seconds of storage time. This defined excitation lead to photoinduced decay signals which, again, showed signs of radiative cooling for $Cu_{6,7}^-$, not, however, for $Cu_{4,5}^-$.

DOI: 10.1103/PhysRevA.94.033407

I. INTRODUCTION

Clusters mark the bridge between atomic systems and condensed matter. The evolution of basic cluster properties from small molecularlike systems towards bulk material comprises crucial information about their geometric and electronic structure. Here, the understanding of new features such as the existence of superatoms [1,2] is of fundamental importance. Especially metal clusters have recently attracted much attention with respect to potential technical applications [3]; examples are biolabeling [4] and catalysis [5]. In the case of the alkali metals like sodium with only one *s* valence electron shell-model calculations allow one to predict fundamental properties like electronic shell closures [6]. Due to their closed *d* shell in combination with one *s* electron, the coinage metals (Au, Ag, Cu) exhibit many similarities to the alkali metals. Although the localized *d* electrons may modify some characteristics, jellium models are often used to describe the electronic shell structure of various metal clusters [7].

In particular copper clusters play an important role in catalysis [8] and bioimaging [9–11]. Although challenging for theoretical approaches due to the localized *d* electrons, numerous calculations on copper clusters have been performed: Their geometry [12–18], absorption spectra [19], and polarizability [20,21] were studied in detail. In addition, many experiments were devoted to Cu clusters, e.g., photoelectron spectroscopy [22–25], determination of the dissociation energies [26,27], and measurements of the polarizability [28]. However, until recently, the radiative cooling of rovibrational highly excited copper clusters has not been investigated. This process is determined by the clusters' infrared active modes and their electronic structures. Thus, it can provide crucial information about the basic characteristics like the cluster structure and electronic states.

To investigate the radiative cooling of negatively charged copper clusters ranging from Cu_4^- to Cu_7^- we have monitored the decay of the highly excited clusters produced in a sputter source. In addition, we employed laser-induced delayed electron emission and fragmentation in a temperature controlled electrostatic ion-beam trap (EIBT) [29,30] at 15 and 300 K, respectively, where the cooling process could be monitored up to several seconds. The different time dependencies of electron emission allowed us to compare the cooling processes of the various cluster sizes.

In the next section the experimental procedure and the apparatus will be discussed. Section III introduces delayed electron emission, cluster fragmentation, and radiative cooling by a state-of-the-art model description. In Sec. IV the experimental results on anionic copper clusters of sizes 4–7 will be presented. The implications of the electron emission and fragmentation signal will be discussed in order to derive information about the radiative cooling process of the various cluster sizes.

II. EXPERIMENTAL PROCEDURE

The measurements were performed with the cryogenic trap for fast ion beams (CTF) [31] device at the Max-Planck-Institut für Kernphysik in Heidelberg. The setup is schematically shown in Fig. 1. Small anionic copper clusters are produced in a caesium ion sputter source, which is known to produce ions in highly excited rovibrational states [32,33]. The continuous ion beam is chopped into bunches of $26-35\ \mu$s, depending on the cluster size, mass selected by a 90° bending magnet, and guided by ion-optical elements towards the EIBT. The trap is attached to a super-fluid helium refrigeration system. Here, it was operated at 15 K and room temperature, i.e., about 300 K, respectively. During cryogenic operation at 15 K the particle densities are equivalent to pressures of 10^{-13} mbar at room temperature [31]. Due to these excellent vacuum conditions the main ion-loss mechanism, i.e., collisions with residual gas molecules, is greatly reduced. Thus, ion beams with kinetic energies of some keV can be stored for several minutes in the cryogenic environment. At room temperature a pressure of below 10^{-10} mbar is reached leading to storage lifetimes of a few seconds.

For ion capturing the entrance mirror is switched from ground to trapping potential after the ion bunch has entered the trapping region of the EIBT. Neutralized clusters and neutral fragments leave the trap on axis and are detected with a microchannel plate detector (MCP) placed behind the annular mirror electrodes on the exit side of the EIBT.

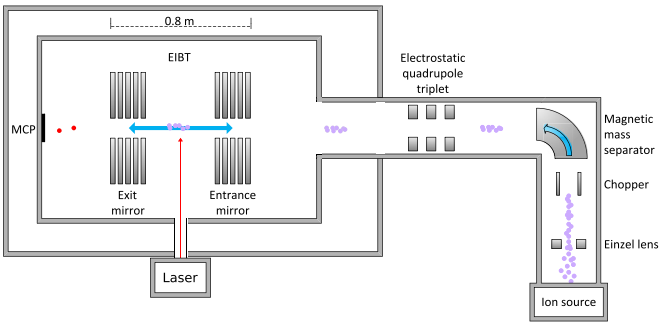

FIG. 1. Schematic view of the CTF setup with ion source, magnetic mass separator, electrostatic guiding elements, the electrostatic ion-beam trap, and the microchannel plate detector (MCP) for neutral particle detection.

Based on the ion current measured with a Faraday cup placed behind the mass separator, the number of injected ions varied roughly between 10 000 (Cu_7^-) and 100 000 (Cu_4^-) depending on the ion species. The experimental cycle was repeated a few thousand times, thus the total number of ions involved in the investigations of a given copper cluster ranged from several 10 millions to billions.

After injection, some ions with sufficiently high internal energy can either emit their excess electron or undergo fragmentation, thus leading to a decreasing rate of neutral products which is observed up to second. This signal will be referred to as the "initial signal." The energy acceptance of the EIBT is about 6000 ± 600 eV, thus ions with mass numbers of the species investigated here are lost from the trap after atom evaporation. The clusters that do not fragment or lose their excess electron remain in the trap and can be excited by a laser pulse. Each excitation is followed by a few milliseconds of increased neutral-product rate. This response will be referred to as the "laser-induced" signal.

A pulsed Nd:YAG laser with a pulse duration of about 15–20 ns and repetition rate of 50 Hz is used to excite the ions in a crossed beam configuration. The laser is operated at $\lambda = 1064$ nm, thus providing photons with an energy of 1.165 eV. After photon absorption the excited clusters may undergo delayed electron detachment, fragmentation or radiative cooling. Direct photodetachment can be ruled out, as the photon energy is even lower than the adiabatic electron affinities listed in Table I and thus lower than the vertical electron affinities. The waist of the laser beam was expanded to a diameter of about 1 cm and its pulse energy was chosen to be sufficiently low (typically 8–10 mJ) ensuring single-photon absorption. Due to the small beam size compared to the geometric trap length and the higher ion density in the mirrors about 1.5 % of the stored ions are in the overlap region. Only a small portion of these ions is expected to absorb a photon.

A typical diagram of MCP signal intensity versus time is shown in Fig. 2. The baseline of the signal in Fig. 2(a) consists of three components. At short times, i.e., up to 0.2 s, the initial decay dominates the signal. After the initial decay is quenched the baseline is caused by neutralization of the clusters in collisions with residual gas molecules in the EIBT. Two seconds after the injection the entrance-mirror potential is switched down to empty the trap. The signal drops to the dark

TABLE I. Published values of the adiabatic electron affinities (EA), the dissociation thresholds D_0 for single atom loss (both in eV), and the polarizability α (in $Å^3$) of Cu_{4-7}^-.

Cluster	Cu_4^-	Cu_5^-	Cu_6^-	Cu_7^-	Ref.
EA	1.40(5)	1.92(5)	1.92(5)	2.10(5)	[22]
EA	1.32(10)	1.82(5)	1.81(10)	1.98(15)	[23]
EA			1.95(5)	2.15(5)	[24]
EA				1.87(8)	[25]
EA[a]	1.37(5)	1.87(4)	1.91(4)	2.05(3)	
D_0	1.93(12)	2.35(12)	2.55(30)	2.87(22)	[27]
α[b]	15.8	15.5	15.2	15.0	

[a]Weighted mean of the literature values.
[b]Linearly extrapolated from experimental data [28].

count rate of the detector. The peaks correspond to the laser pulses. Figure 2(b) shows a zoom of the time axis by a factor of 2000 of the signal just after laser excitation. Due to low statistics the signal of the first 20 laser shots of Fig. 2(a) were summed up, i.e., the signals within the gray area of Fig. 2(a). Zero time in this figure represents the time of the maximum count number of the first bunch of neutrals arriving at the detector.

The laser pulse excites a subset of the ions which are present in the laser crossing region at the moment of the pulse. The peaks in Fig. 2(b) correspond to those neutrals produced as the photoexcited ions move toward the detector during their oscillatory motion in the ion trap. Since the neutral production occurs in flight at high ion velocity, the arrival times at the detector essentially reflect the time-of-flight spread resulting from the distribution of distances of the initially excited ions to the detector. The oscillation phases of the ions in the EIBT are essentially random at the laser pulse time, thus, half of the excited ions move toward the detector, while the other half

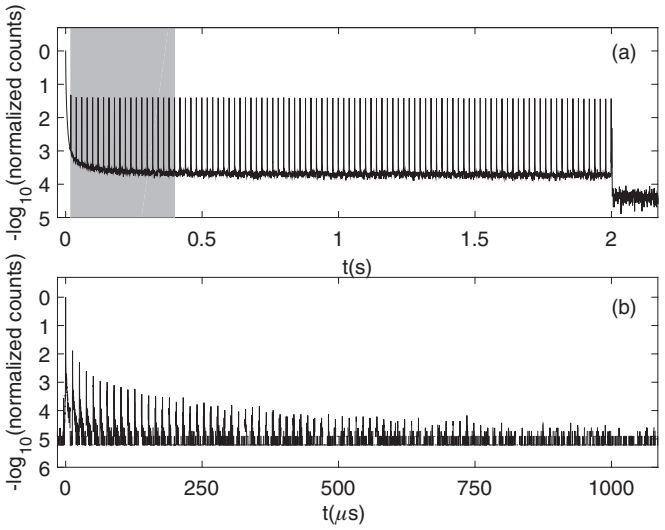

FIG. 2. MCP signal of neutralized Cu_4^- clusters as a function of storage time. (a) Signal intensity for two seconds of storage employing laser excitation with a repetition rate of 50 Hz. (b) Zoomed time axis and summation of 20 laser-shot signals, highlighted by the gray area in (a).

TABLE II. Revolution frequency f and period T of Cu_{4-7}^- extracted from the initial signal.

Cluster	Cu_4^-	Cu_5^-	Cu_6^-	Cu_7^-
f/kHz	39.5(2)	35.3(2)	32.2(1)	29.8(1)
T/μs	25.3(2)	28.3(2)	31.1(1)	33.6(1)

move away from it. Corresponding to these two ensembles, the pulses are spaced by half an oscillation period. The revolution frequencies f and period T for the different investigated copper clusters are listed in Table II.

Since the neutral production rate decreases as a function of time following the laser shot, the amplitudes of these pulses decrease [Fig. 2(b)]. Due to the high rate in the first peak, saturation effects of the read-out electronics of the detector might falsify the measurement. Thus, in the analysis of the time dependence, all pulses except the first one after the excitation are considered. The uncertainty due to the finite overlap area with the laser can be neglected in the analysis.

III. STATISTICAL MODEL CALCULATIONS

To evaluate the observed time dependencies of the initial and the laser-induced neutral product signals, calculations within a statistical description of the occupation of the clusters energy levels were performed. Emitting an electron with energy ϵ from the parent cluster with vibrational energy E leads to a daughter cluster with the vibrational energy $E - EA - \epsilon$, where EA is the adiabatic electron affinity of the neutral cluster. Employing a detailed balance approach the rate of this process can be deduced from the electron-capture cross section $\sigma(\epsilon)$ as given in [34,35]:

$$k_{\mathrm{det}}(E) = \int \frac{2m}{\pi^2\hbar^3}\epsilon\sigma(\epsilon)\frac{\rho_d(E-EA-\epsilon)}{\rho_p(E)}d\epsilon. \qquad (1)$$

Here, m is the reduced mass of the neutral cluster and the emitted electron, and ρ_d and ρ_p are the vibrational densities of states of the neutral daughter and anionic parent cluster, respectively. The electron-attachment cross section of the neutral cluster [35],

$$\sigma = \pi\sqrt{\frac{2\,\alpha\,e^2}{\epsilon}}, \qquad (2)$$

is deduced from the Langevin cross section, assuming full sticking probability for the electron in case it overcomes the angular momentum barrier of the neutral cluster. α is the polarizability of the involved neutral cluster and e the electron charge. This approximation can significantly overestimate the attachment cross section, so that the determined rate $k_{\mathrm{det}}(E)$ represents an upper limit. The rotational angular momentum quantum number J_p and J_d of the parent and daughter cluster is neglected in this calculation. This is justified as an approximation since the electron can only take a small amount or even no rotational quanta. Assuming $J_d = J_p$ the shift of the detachment threshold by the rotational excitation is given by $(B_p - B_d)J_p(J_p + 1)$. B_p and B_d are the rotational constant of the parent and daughter clusters, respectively. Since in our case $B_d \approx B_p$, we neglect the difference completely in the following and thus, in the analysis we will assume the detachment rate to be independent of the initial rotational quantum number J_p [34].

For the fragmentation process, however, the difference in the rotational constants of parent and daughter clusters is of major importance. In first approximation the shape of the parent and the daughter clusters is assumed to be spherical. In addition, only the evaporation of a single neutral atom is considered. For the fragmentation of a cluster with vibrational excitation E and a rotational state J_p, we follow phase-space theory [36]:

$$k_{\mathrm{frag}}(E,J_p) = g\sum_{J_d=0}^{J_d=\max}\int_{\epsilon_d^{\min}}^{\epsilon_d^{\max}}\frac{T(J_p,J_d,\epsilon_d)}{2J_p+1}\frac{\rho_d(E+B_pJ_p(J_p+1)-D_0-B_dJ_d(J_d+1)-\epsilon_d)}{h\rho_p(E)}d\epsilon_d. \qquad (3)$$

Here, g is the fragmentation channel degeneracy and ϵ_d the sum of the translational and rotational energy of the daughter particle. In this process, the rotational quantum number can change a lot and the probabilities for different final rotational states J_d have to be summed up. D_0 denotes the fragmentation threshold. $T(J_p,J_d,\epsilon_d)$ is the number of available angular momentum states for given J_p, J_d, and ϵ_d. More details can be found in [37]. B_p and B_d are calculated by a density-functional theory approach and are listed in Table III. To approximate the cluster structure by a sphere the mean over the rotational constants in the three directions of space is used. The large scattering of the rotational constants in the direction of space results in accordingly large uncertainties.

TABLE III. Rotational constants B_n for clusters Cu_n. For electron detachment $B_p = B_d = B_n$ is used, for the fragmentation process $B_p = B_n$ and $B_d = B_{n-1}$.

n	3	4	5	6	7
B_n/μeV	9.5(40)	5.9(44)	3.3(24)	2.6(7)	2.0(5)

The required density of states can be derived from a harmonic approximation by use of an algorithm from Beyer and Swinehart [38]. The vibrational frequencies are similar to the rotational constants derived by a density-function theory, described in [12]. The published values of the EA derived by photoelectron spectroscopy, their weighted averages, and the experimental values for D_0 are listed in Table I.

In Eqs. (2) and (3) the polarizabilities of the neutral copper atom and involved clusters are needed. Up to now no experimental data for the investigated cluster sizes are available, but the polarizabilities of larger copper clusters ($n = 9...61$) have been measured [28]. These experimental data differ significantly from theoretically derived values [20].

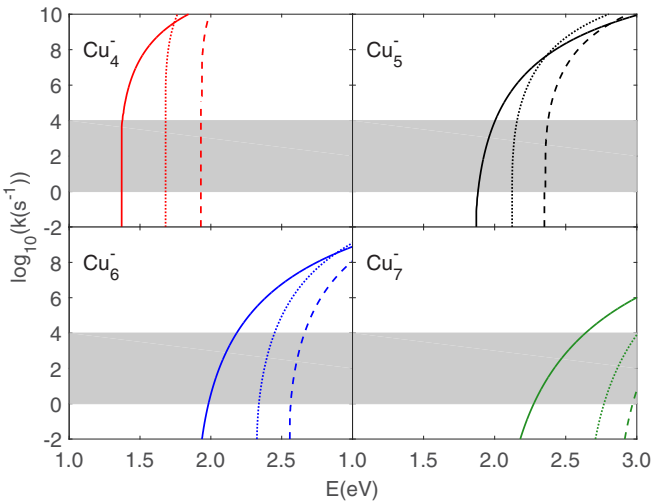

FIG. 3. Calculated decay rates for electron detachment (solid lines) and fragmentation (dashed and dotted lines) of Cu_{4-7}^- in dependence of the internal vibrational energy E. Dashed lines represent an angular momentum of $J = 0$; dotted lines represent the J state with highest population for $T_{rot} = 3000$ K (J=212, 280, 315, 361 for Cu_{4-7}^-). The gray areas indicate rates to which the measurements are sensitive, namely from $k = 1\,s^{-1}$ to $k = 10\,000\,s^{-1}$.

Thus, instead of using calculated values for the polarizability the experimental values per atom from cluster size 45 to 9 were extrapolated linearly to the cluster sizes of interest leading to values between 15 and 16 Å^3. The calculated detachment and fragmentation rates of the investigated cluster species are shown in Fig. 3.

In general, these decay rates are overestimated for two reasons: First, Eq. (2) only describes the cross section with which an electron colliding with a neutral cluster can enter the inner region of the cluster. Thus, for the capture cross section Eq. (2) has to be reduced by a sticking probability [34]. Second, potential anharmonicities lead to an underestimation of the density of vibrational states, due to a reduced spacing between higher vibrational levels. This is more pronounced in the denominator than in the numerator of Eqs. (1) and (3), where the energy is increased by EA and D_0.

Beside the destructive detachment and fragmentation processes the internal energy of the clusters can be reduced by photon emission [39–43]. The rate for photon emission k_{rad} can be derived [44] by detailed balance as

$$k_{rad} = \int_0^{E/h} \frac{8\pi\nu^2}{c^2}\sigma(E - h\nu, h\nu)\frac{\rho(E - h\nu)}{\rho(E)}d\nu, \quad (4)$$

with c being the speed of light, $h\nu$ the energy of the emitted photon, and $\sigma(E - h\nu, h\nu)$ the cross section for absorption of a photon of energy $h\nu$ by a cluster with internal energy $E - h\nu$. There are no literature values for $\sigma(E - h\nu, h\nu)$, but since the photoabsorption is likely to change only slowly with energy, we assume the photon-emission rate to depend only weakly on E for $E \approx EA$.

If the detachment and fragmentation rates k_{det} and k_{frag} as well as the photon emission rate k_{rad} are known, the decay curves, i.e., the decays per time interval as a function of time, can be calculated for any given vibrational and rotational energy distributions $m(E)$ and $n(J)$:

$$R(t) = \sum_{J=0}^{\infty}\int_0^{\infty} n(J)m(E)(k_{det}(E) + k_{frag}(E,J)) \times e^{-(k_{det}(E)+k_{frag}(E,J)+k_{rad}(E))t}\,dE. \quad (5)$$

Due to the small heat capacities of the clusters and the rapidly increasing detachment and fragmentation rates in dependence of the internal energy, a single emitted photon already quenches the decay, and thus reduces directly the number of excited clusters. But in contrast to the detachment and fragmentation processes no detectable neutral particle is produced. As a consequence, k_{rad} contributes exclusively to the exponent in Eq. (5). Only a small fraction of the energy distribution is involved in the decay. Due to the weak energy dependence of k_{rad} around EA, we neglect the energy dependence within the involved fraction of the energy distribution and keep k_{rad} as a constant in Eq. (5).

The summation over various exponentials in Eq. (5) results in a power law in time. The power law exponent κ is usually on the order of -1. Due to the small heat capacity of the clusters and its shape of the energy distribution the power is modified [35]. If the slope of the energy distribution $m(E)$ at the relevant energies is positive, the absolute value of the power law exponent is increased and vice versa for a negative slope [35]. Due to the depletion of long-lived states by radiative cooling or if no longer living states are populated or existing the decay curve will be quenching and start to deviate from the power law. The decay curve can be approximated by [45]

$$R = \frac{R_0\,(t/\tau)^{\delta}}{e^{t/\tau} - 1}. \quad (6)$$

Here the exponent of the power law in time is $\delta - 1$. Around τ the curve starts to deviate towards an exponential decay with $\exp(-t/\tau)$.

IV. EXPERIMENTAL RESULTS

In the present experiments the anionic copper clusters are produced in highly excited rovibrational states [32,33]. Some of the clusters have sufficient vibrational and rotational energies to decay spontaneously (i.e., without further excitation such as photoirradiation) either by electron detachment or by cluster fragmentation (Sec. IV A). The remaining clusters are subsequently excited by a laser pulse in order to reintroduce internal energy causing further electron detachment and fragmentation. The averaged time patterns of the decay signals [shown in Fig. 2(b)] are analyzed as a function of the time of the laser pulse after production of the clusters and capturing in the EIBT [Fig. 2(a)] to study slowly proceeding cooling processes of the cluster systems (Sec. IV B).

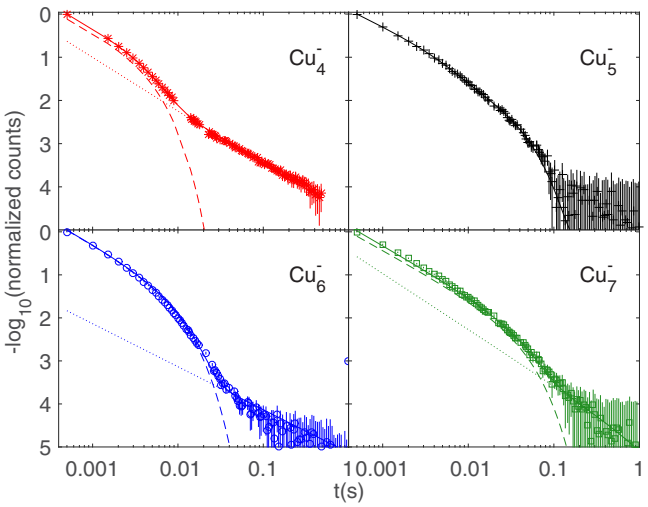

FIG. 4. Counts of neutralized or fragmented copper clusters within the first second of storage for cluster sizes 4–7 with the CTF at $T = 15$ K. The solid lines are the summation over two power laws of Eq. (6) to guide the eyes; the dashed (dotted) line represents only the first (second) of the two components.

A. Spontaneous decay of clusters produced in highly excited rovibrational states

Figure 4 shows the decay curves (i.e., the "initial signal") of Cu_{4-7}^- with the EIBT operated at $T = 15$ K. Due to the excellent vacuum conditions during cryogenic operation the background count rate is extremely low. Thus, the decays can be followed up to several hundred milliseconds. Except for the lower collisional background, no differences between cryogenic and warm operation are expected, since the clusters have temperatures above 1000 K and on the observed time scales radiative energy exchange with the vacuum chamber due to black body radiation can be neglected.

With the exception of Cu_5^-, where the statistics are too low to be conclusive, all decay curves exhibit two components. The second component becomes observable only when the first one quenches. Both components follow a power law in time and thus can be fitted with Eq. (6). The first component quenches completely, while the second component could not be followed sufficiently long to observe a quenching, if it occurs at all. The observation of the second component reveals the presence of a second decay process for a subclass of clusters.

In the past two decades many studies were performed on the decay of small, rovibrationally excited molecular and cluster anions such as large fullerenes [46,47], SF_6^- [48], $Al_{4,5}^-$ [49], small anionic copper clusters [50], and anionic metal dimers [51]. All these studies demonstrated that the nonexponential decay curves follow a power law in time. In [50] a decay revealing a two-component power law was reported.

The first component can be well described with the statistical model and the calculated decay rates in Eq. (5). Since electron detachment has a lower threshold compared to fragmentation it will occur preferentially, and we assign the first component to this process. It is generated by superposing exponential decays of various populated excited states with a distribution according to the high internal temperature with different decay constants [34,35]. There are two possible explanations for its quenching: Either (i) radiative cooling depletes the population of the decaying states or (ii) the low decay rates of the lowest populated decaying states terminate the power law behavior. The times when the curves start to deviate from the power law are on the order of the inverse of the decay rates of the states lying closest to the threshold. For Cu_{5-7}^- the calculated decay rates of states around the EA as well as their threshold fragmentation rates are too low to explain the quenching. For these clusters there are states with life times much longer than the observed quenching (Fig. 3). Thus, the decay would have to follow a power law much longer, if these states were not depopulated by radiative cooling. In the case of Cu_4^- the calculated rates are too high to even reproduce the first component of the decay pattern displayed in Fig. 4. We conclude that the observed quenching should be due to radiative decay in these cases.

TABLE IV. The cooling rates for fitting the initial decay with Eq. (5) for clusters Cu_n.

n	4	5	6	7
k_{rad} / s^{-1}	–	44	190	43

We employed Eq. (5) to fit the data assuming an *a priori* canonical energy distribution $m(E) = \rho_p(E)\exp(-E/k_BT)$. A simple power law fitted to the later data points approximated the second component of the initial decay. Thus, for fitting the first component only the temperature T of the decaying ensemble as well as the energy independent radiative cooling rate k_{rad} [see discussion following Eq. (4)] remain as free parameters. The fitted cooling rates are listed in Table IV. In case of Cu_4^- no fit could be performed, since—as discussed above—the calculated detachment rates are too high. The extracted values of the temperature T are about 1000 K, which is below the expectations. This is most likely due to the overestimation of the detachment rates (see Sec. III). The part of the energy distribution involved in the decay is thereby shifted, resulting in lower extracted temperature values. The fitted cooling rates k_{rad} are comparable to results reported for other anionic molecular systems such as SF_6^- [48] and amino acids [45]. But they are slightly smaller than the measured rates for $Al_{4,5}^-$ [49].

The second component of the decay curves cannot be fitted with Eq. (5), since the introduction of a single radiative cooling rate k_{rad} to fit the quenching of the first component suppresses the second component as well. Thus, the clusters contributing to the second component must be affected differently by radiative cooling. Possible reasons will be discussed in the following. First, fragmentation could explain the second component. Due to angular momentum conservation the rotational energy can only be accessed in fragmentation, but not in electron detachment. Therefore, rotationally excited clusters can fragment even if the vibrational energy is lower than the dissociation threshold. In Fig. 3 such an effective threshold for fragmentation can be seen. Nevertheless, the calculated fragmentation and detachment rates demonstrate even for very high rotational temperatures that fragmentation can only compete with electron detachment for internal energies far above the

EA. But then the decay would be much faster than the time scales accessible in this experiment. Thus, for fragmentation rotational temperatures above 3000 K have to be considered, which is implausible. Alternatively, the dissociation thresholds of Cu clusters [27] are overestimated by about half an eV or vice versa the EA is underestimated. However, we cannot comment on the accuracy of the measurements in [22–25,27]. If dissociation can compete with electron detachment on experimental time scales, a wide range of populated J states would result in a wide range of vibrational energies involved in the decay. Thus, the energy dependence of k_{rad} could not be neglected anymore and quenching at later times could be possible.

A second explanation for the second component in the decay curves might be the storage of internal energy in a metastable electronic state. In this case the vibrational energy needed for electron detachment is lower and thus the rate for photon emission is lower and the decay curve quenches at later time. There is no information about the existence of such metastable states.

In [50] the decay of Cu^-_{3-6} produced in a similar ion source was investigated. There, two components were observed for the decay of $Cu^-_{4,5}$ but not for Cu^-_6. For Cu^-_4 the decay was followed up to 2 s and a quenching of the second component was also observed. The decay curves of Cu^-_4 in [50] and the one presented in this article are very similar in general, but also show distinct differences between each other in some properties. The time the first component quenches is all about the same in both curves, but the exponents of the two power law components differ. The fit of two added power laws of Eq. (6) to the data results in $\delta - 1 = -0.94$ for the first component and $\delta - 1 = -1.24$ for the second component, respectively. The first component of the decay curve shown in [50] seems to be steeper, whereas the second component tends to be flatter compared to our measurements. Because the quenching time of the first component depends on the radiative cooling rate, an intrinsic property of the cluster, it is expected to be identical in both experiments. According to Eq. (5) the decay curves depend strongly on the energy distribution of the clusters. Thus, the differences in the measured decay curves may be due to differences in the energy distributions of the ion ensembles caused by the production processes. Even though the same kind of ion source was used (caesium ion sputter source) the applied parameters such as the acceleration voltage for the caesium ions will affect the internal energy distribution [48]. In [50] the explanation suggested for the observation of two decays was the presence of two different shape isomers, a linear one, which cools radiatively much more slowly than the second one, a two-dimensional structure, and thus the second component of the decay quenches later. Different isomers for anionic copper clusters were predicted in several theoretical studies [12,16,18]. Considering the wide energy distribution produced by the ion source the presence of different isomers is indeed likely. Nevertheless, the observation of electron detachment without further excitation is a clear proof of a high internal energy of the clusters reaching at least EA. Assuming a heat capacity of $6\,k_B$ for Cu^-_4, this would correspond to a temperature of around 2500 K. Thus, the second isomer would have to show a high stability in spite of a strong internal excitation. Further studies appear necessary in order to show the sufficient stability of excited isomers under these conditions.

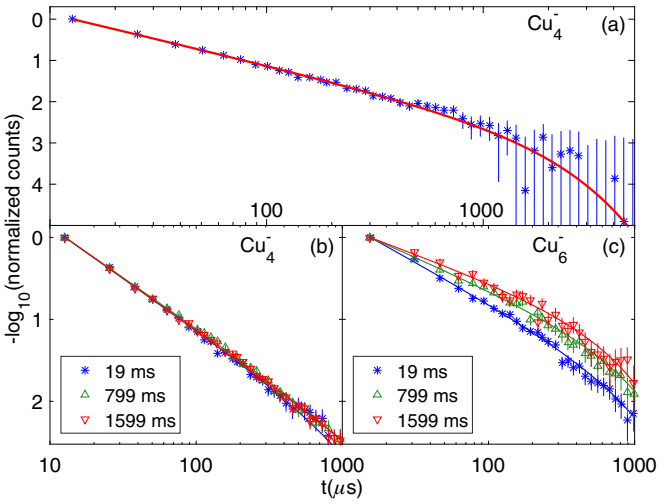

FIG. 5. (a) Integrated number of counts versus time after laser excitation of Cu^-_4. Due to low statistics 20 consecutive laser shots are summed up. The red line is a fit of Eq. (6) to the data. In (b) and (c) the decay curves for Cu^-_4 and Cu^-_6, respectively, after laser excitation are shown for various storage times. Again, 20 consecutive laser shots are summed up due to low statistics and the lines are fits of Eq. (6). All data were measured with the EIBT at 15 K.

B. Laser-induced delayed decay

The laser-induced neutral product rates as a function of time after laser excitation are shown in Fig. 5. As explained in Sec. II, these rates correspond to the sum of all recorded events within time windows centered at integer multiples of half of the revolution period T of the stored ions (see Table II). As in Fig. 2(b), the signals from 20 consecutive laser pulses, corresponding to 0.4 s storage time, are summed up. Typical decay curves for Cu^-_4 and Cu^-_6 are plotted in Figs. 5(b) and 5(c). In case of Cu^-_4 the spectra at different storage times remain identical within their uncertainties, while the slopes of the spectra measured for Cu^-_6 are clearly storage time dependent.

For further analysis, the summed signal for each storage time interval of 200 or 400 ms, depending on the statistics, is fitted to Eq. (6) and the power law exponent $\kappa = \delta - 1$ is derived. The time intervals correspond to 10 and 20 laser shots, respectively. The time dependencies of κ are plotted in Fig. 6 for the investigated cluster sizes and trap temperatures. No storage time dependence is seen for Cu^-_4 and Cu^-_5, where κ is near -1.2 and -1, respectively. In contrast, a clear change of κ over the first $\approx$2 s can be found for Cu^-_6 and Cu^-_7, when κ increases from ≈ -1.2 to below -0.8 for Cu^-_6 and from ≈ -1 to below -0.8 for Cu^-_7. At later storage times, κ seems to be almost constant. Measurements were performed at CTF temperatures of 15 K (Fig. 6 left) and 300 K (Fig. 6 right). The data taken at 300 K and 15 K are identical within the uncertainties, except for Cu^-_6 where the steady state seems to be reached a little earlier.

Several comparable studies on laser-induced decay of ions were performed in the past. The laser-induced decays

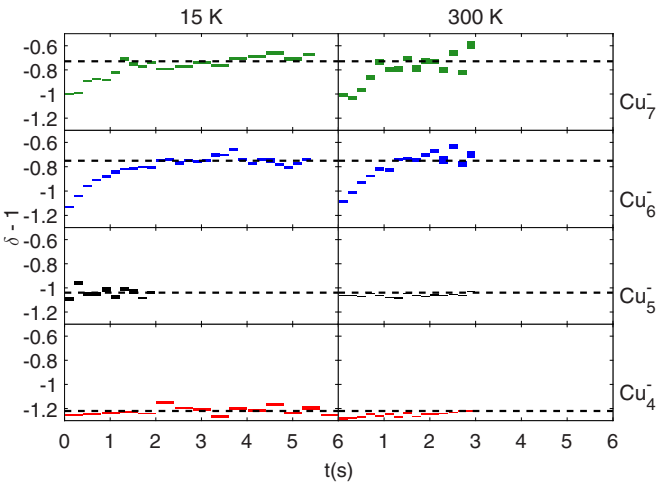

FIG. 6. The extracted power of Eq. (6) fitted to the decay curves after laser excitation in dependence of storage time is plotted for clusters Cu^-_{4-7}. Due to statistical reasons the number of laser shots, which were summed up, is not identical for all cluster sizes and the time over which laser shots were summed up is indicated by the width of the boxes, whereas the hight indicates the uncertainty of the fit. The temperature of the trap has been kept at 10 K (left) and 300 K (right), respectively. Dashed lines mark the average power of decay curves taken at 15 K after reaching a steady state.

of anionic aluminum [37,40,52] and carbon [42,43,53,54] clusters as well as the decay of larger carbon bearing molecules [41,55] were investigated. For most of these studies the decay curve follows a power law in time after excitation. Only for C_4^- and C_6^- an exponential decay was measured [43,54], which can be explained by a large radiative cooling rate k_{rad} dominating the decay. If a power law was observed, its shape changed with storage time, indicating a cooling in the critical region of the energy distribution of the stored ion ensemble. In case of Al_4^- the cooling could be followed below room temperature, but comparable to $Cu^-_{6,7}$ it stopped before equilibrium with the 10-K environment was reached [52]. Only for anionic zinc phthalocyanine ($C_{32}H_{16}N_8Zn^-$) a storage time independent laser-induced power-law decay was observed [55]. These findings are similar to the present data of $Cu^-_{4,5}$, but the authors of [55] deduced a cooling of the ensemble from the dependence of the signal strength on the laser power. Nevertheless, the measurements differ on some points: For Cu_4^- (Cu_5^-) only 6 (9) vibrational degrees of freedom are involved. In case of $C_{32}H_{16}N_8Zn^-$ the number is much larger (165). As a consequence, the detachment rate k_{det} increases much slower with energy and the involved energy region is much wider. In addition, the decay was induced by multiphoton absorption in contrast to single photon absorption in our case.

As discussed in Sec. III, the exponent of the decay curve carries a signature of the slope of the vibrational energy distribution $m(E)$ in the energy region $E \gtrsim EA$ where the inverse decay rates $k_{\mathrm{det}}^{-1}(E)$ are in the time range of the recorded laser-induced spectra, e.g., between $\approx 10\,\mu$s and ≈ 1 ms ($\log_{10}(k_{\mathrm{det}} \times \mathrm{s}) \approx 2...4$); see Fig. 5. In the following this will be referred to as the energy region of interest.

Several previous studies were devoted to the extraction of the energy distribution from delayed electron-detachment experiments. In [40,52] a Boltzmann distribution was adopted to derive a temperature from the measured decay curve, in [41] a Gaussian distribution was used to derive the energy distribution and in [42] the normalized numbers of delayed electron detachment events for different photon energies were compared. Here, we extract direct information on the shape of the energy distribution using Eq. (5) to fit the decay curves. To this end, it is assumed that the absorption of a laser photon of energy E_{ph} shifts the energy of a cluster from E' to $E = E' + E_{\mathrm{ph}}$. The shifted distribution $m(E) = m'(E')$ is then inserted into Eq. (5) to perform a fit of the measured laser-induced decay.

We analyze the results for Cu_6^-, where the energy region of interest ranges from 2.055 to 2.305 eV. This corresponds to an energy interval ranging from 0.885 to 1.135 eV before the laser excitation. Due to the overestimation of the detachment rates (see Sec. III) the region of interest could be underestimated and lie slightly higher. However, we assume that the shape of the $k_{\mathrm{det}}(E)$ dependence still sufficiently holds for the analysis of the energy distribution. We subdivided the region of interest into five equally sized bins for which contributions to $m'(E')$ are determined by a fit to the data. The laser-induced signals were summed up into six time intervals with different lengths, ranging from 0.3 to 1.7 s. The results are shown in Fig. 7. The comparison with calculated thermal distributions suggests that cooling proceeds from $T \approx 1100\,K$ at short times (0.02–0.3 s) to $T \approx 700$ K at later storage times (3.7−5.5 s).

The constant exponent of the curves for $Cu^-_{4,5}$ suggests that the energy distribution in the region of interest does not change for these clusters. This is not in contradiction to the observation of the electron emission following the ion production, where the quenching of the decay curves was linked to a radiative cooling process in case of Cu^-_{5-7}, because both processes probe different parts of the ions' energy distribution [see Fig. 7(a)]. The varying power of the decay curves of $Cu^-_{6,7}$ represents a storage-time-dependent change of the energy distribution at lower energies $E \approx 1$ eV. Before cooling the hot ensemble indicated by the detachment of the ions without laser excitation leads to a rising, flat or only slowly decreasing energy distribution in the region of interest. Since the sensitive region (≈ 1 eV) is far above the vibrational ground state, predominantly lower-energy clusters are expected after cooling. Thus, for a cooling ensemble a reduction of the absolute value of the power law exponent is expected, as discussed in Sec. III. This is in agreement with the measurements presented in Fig. 6.

The presence of the initial decay without excitation as discussed in Sec. IV A indicates an initially hot ensemble. The temperature of 1100 K estimated for Cu_6^- for short storage times is in agreement with this finding. The fast decrease of temperature is comparable to what was observed for cooling of other small metal clusters [39,40,52]. The stopping or dramatic slowing down of the cooling indicates a strong dependence of the radiative cooling rate on the internal energy.

Even for Cu_6^- and Cu_7^- the observed cooling process does not lead to an equilibrium of the cluster temperature with the environment. The photon energy $E_{\mathrm{Ph}} = 1.165$ eV is far below the EA and D_0. Furthermore, at a temperature of 15 K vibrational energies of the order of $E_{\mathrm{vib}} = 10$ meV are expected. The sum $E_{\mathrm{Ph}} + E_{\mathrm{vib}}$ is insufficient for delayed

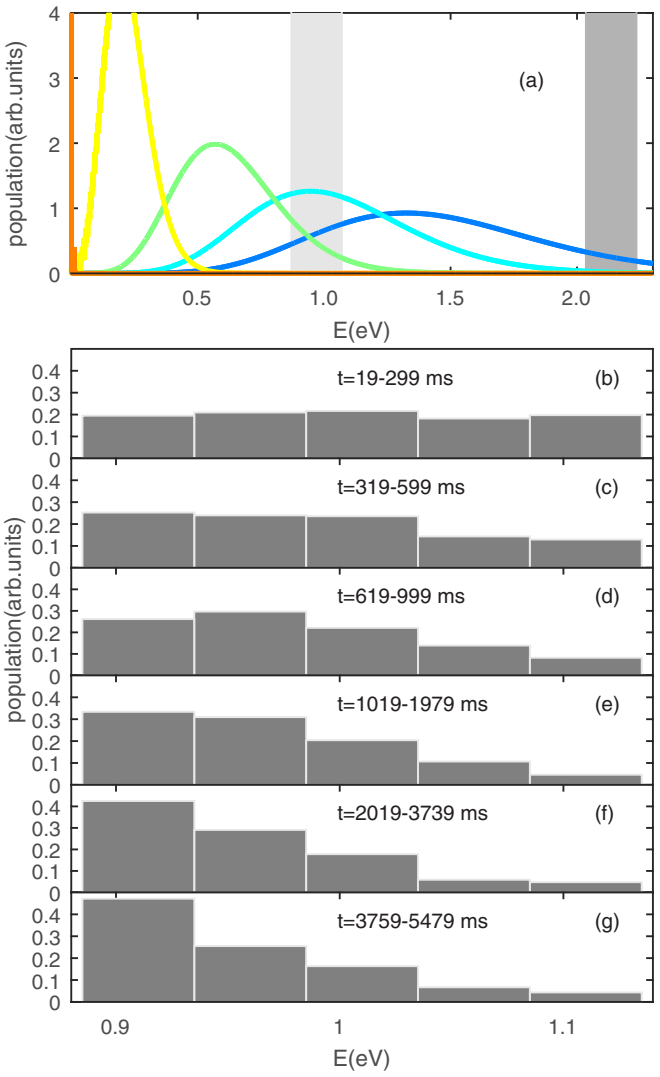

FIG. 7. (a) Canonical energy distributions $m(E) = \rho_p(E)\exp(-E/(k_B T))$ for different temperatures (15 K orange, 300 K yellow, 700 K green, 1100 K cyan, and 1500 K blue) for Cu_6^-. The dark gray area is the part of the energy distribution that undergoes electron detachment on time scales to which the measurements are sensitive. The light gray area is shifted by 1.165 eV and thus represents the part of the energy distribution prior laser excitation the measurements are sensitive to. (b)–(f) Energy distributions for Cu_6^- for different storage time intervals and the EIBT at 15 K. The shown populations are normalized to 1. See text for further details.

electron detachment or fragmentation of even highly rotationally excited clusters. In addition, the results of the measurements at 15 and 300 K are identical within the uncertainties for $n = 4,5,7$, while for $n = 6$ at least the final value of the power-law exponent seems to be independent of the trap temperature (see Fig. 6). In case of Cu_6^- and Cu_7^- a steady state seems to be reached within the first two seconds, further cooling becoming much smaller (if existing at all) taking the present data set. Small deviations between the results obtained at 15 and 300 K for Cu_4^- and Cu_5^- might be explained by minor variations in the ion-production process. A high temperature infrared light emitter prohibiting equilibration with the vacuum chamber cannot have strong effects, as the CTF at 15 K has demonstrated the radiative cooling of Al_4^- below 300 K [52].

The radiative energy emission can be driven by vibrational infrared emission as well as by electronic excitations [47]. In case of metal clusters the vibrational modes are known for their low infrared activities. Thus, energy loss by vibrational infrared emission is inefficient. The emission by electronic excitations depends on the energy E_{elec} of the involved electronic state or plasmon. Electronic excitations can only contribute to the radiative cooling process if $E > E_{\mathrm{elec}}$. The photon emission through electronic states can be much more efficient than infrared vibrational emission [47], resulting in a strong energy dependence of k_{rad}. The unchanged energy distribution in the region of interest for $Cu_{4,5}^-$ might be linked to the low efficiency of vibrational infrared emission and the absence of electronic states in the specific energy region. In case of Cu_4^-, ions with an internal energy of about 200 meV are probed, while for Cu_5^- the internal energy of the ions is about 700–850 meV prior to laser excitation. There are no reliable predictions about the electronic states in these energy regions. The observed cooling process of $Cu_{6,7}^-$ cannot be explained by a combination of vibrational infrared emission and fast, effective cooling via one electronic state. In this case, all ions with vibrational energy above a certain threshold would be cooling via this electronic state. Since we can observe a change in the decay curves after laser excitation for $Cu_{6,7}^-$ such a threshold might be in the region of interest. Therefore, with a sharp onset of the electronic decay as a function of E, the energy distribution in the region of interest should develop into a steplike function, since all states which can undergo the electronic cooling would deplete, in contrast to our observations (compare Fig. 7).

It is not clear whether the stopped or drastically slowed cooling can be linked to the process causing the second components in the initial decay signals. However, even if the second component is caused by fragmentation and the laser-induced decay is dominated by fragmentation, a decay curve unaffected by the ion-ensemble temperature prior to laser excitation is not reasonable. In contrast to the vibrational cooling the rotational cooling takes place on much longer time scales, because each photon can reduce the angular momentum by only $1\hbar$. Although the rotational energy can be partly accessed in fragmentation, the fragmentation rates still depend strongly on the vibrational energy. Thus, a significant difference of the decay of clusters in an environment of 15 and 300 K is expected, in contrast to the observations.

On the other hand, different isomers or energy storage in metastable electronic states can explain the observations at least partly. Assuming there are both slowly as well as fast cooling ion ensembles, the evolution of the laser-induced decay curves represents the evolution of the mixed ensemble. The initial change of the power law exponent for Cu_6^- and Cu_7^- thus reflects the change in the fast cooling ensemble, whereas the signal level of $\delta - 1$ at later times can be understood as being due to the slowly cooling ensemble, while the fast cooling ensemble does not contribute to the energy region of interest, anymore.

For Cu_4^- and Cu_5^- the stable level of $\delta - 1$ might reflect the slowly cooling ensemble, nevertheless the first component of the initial decay is still observable for Cu_4^- at the time the

laser is fired the first time, and thus, in contradiction to the observation, a changing energy ensemble is expected. Therefore, the assumption of two differently cooling ensembles cannot explain the observations for Cu_4^-

V. CONCLUSION AND OUTLOOK

The decay of highly excited anionic copper clusters produced in a sputter source as well as laser-induced decay of these clusters after extended storage in a cryogenic electrostatic ion-beam trap were observed for cluster sizes ranging from four to seven atoms. The decay after ion production was followed for several hundreds of milliseconds and consists of two components, where the first one can be assigned to delayed electron emission. The second component was discussed, but could not be linked with certainty to any source.

For $Cu_{4,5}^-$ clusters radiative cooling apparently caused the observed quenching of the decay after ion production, while it did not lead to changes in the shape of the energy distribution for the lower energies probed by the laser. In the case of $Cu_{6,7}^-$ fast radiative cooling can be detected in the first two seconds of storage. However, this cooling stops or slows down considerably before equilibrium is reached with the trap´s 15 K or 300 K environments. For a deeper understanding of the involved processes a variation of the probed energy region would be necessary, which could be obtained by changing the laser wavelength. To determine the final cluster temperature comparative measurements with rovibrationally cold ions are of interest.

ACKNOWLEDGMENTS

We thank D. Schwalm for helpful discussions. We acknowledge financial support from the Max-Planck Society and the Max-Planck Förderstiftung.

[1] S. N. Khanna and P. Jena, Phys. Rev. Lett. **69**, 1664 (1992).
[2] A. W. Castleman Jr., J. Phys. Chem. Lett. **2**, 1062 (2011).
[3] Y. Lu and W. Chen, Chem. Soc. Rev. **41**, 3594 (2012).
[4] M. A. H. Muhammed, P. K. Verma, S. K. Pal, R. C. ArunKumar, S. Paul, R. V. Omkumar, and T. Pradeep, Chem. Eur. J. **15**, 10110 (2009).
[5] A. Taketoshi and M. Haruta, Chem. Lett. **43**, 380 (2014).
[6] W. D. Knight, K. Clemenger, W. A. de Heer, W. A. Saunders, M. Y. Chou, and M. L. Cohen, Phys. Rev. Lett. **52**, 2141 (1984).
[7] M. Brack, Rev. Mod. Phys. **65**, 677 (1993).
[8] W. Wei, Y. Lu, W. Chen, and S. Chen, J. Am. Chem. Soc. **133**, 2060 (2011).
[9] L. Zhang and E. Wang, Nano Today **9**, 132 (2014).
[10] M. J. Barthel, I. Angeloni, A. Petrelli, T. Avellini, A. Scarpellini, G. Bertoni, A. Armirotti, I. Moreels, and T. Pellegrino, ACS Nano **9**, 11886 (2015).
[11] L. Jin, Z. Zhang, A. Tang, C. Li, and Y. Shen, Biosens. Bioelectron. **79**, 98 (2016).
[12] G. Guzmán-Ramírez, F. Aguilera-Granja, and J. Robles, Eur. Phys. J. D **57**, 49 (2010).
[13] B. H. Cogollo-Olivo, N. Seriani, and J. A. Montoya, Chem. Phys. **461**, 20 (2015).
[14] U. Lammers and G. Borstel, Phys. Rev. B **49**, 17360 (1994).
[15] M. Yang, K. A. Jackson, C. Koehler, T. Frauenheim, and J. Jellinek, J. Chem. Phys. **124**, 024308 (2006).
[16] E. M. Fernández, J. M. Soler, I. L. Garzón, and L. C. Balbás, Phys. Rev. B **70**, 165403 (2004).
[17] K. Jug, B. Zimmermann, P. Calaminici, and A. M. Köster, J. Chem. Phys. **116**, 4497 (2002).
[18] P. Calaminici, A. M. Köster, N. Russo, and D. R. Salahub, J. Chem. Phys. **105**, 9546 (1996).
[19] K. Baishya, J. C. Idrobo, Serdar Öğüt, M. Yang, K. A. Jackson, and J. Jellinek, Phys. Rev. B **83**, 245402 (2011).
[20] M. Yang and K. A. Jackson, J. Chem. Phy. **122**, 184317 (2005).
[21] P. Calaminici, A. M. Köster, A. Vela, and K. Jug, J. Chem. Phys. **113**, 2199 (2000).
[22] D. G. Leopold, J. Ho, and W. C. Lineberger, J. Chem. Phys. **86**, 1715 (1987).
[23] J. Ho, K. M. Ervin, and W. C. Lineberger, J. Chem. Phys. **93**, 6987 (1990).
[24] C. L. Pettiette, S. H. Yang, M. J. Craycraft, J. Conceicao, R. T. Laaksonen, O. Cheshnovsky, and R. E. Smalley, J. Chem. Phys. **88**, 5377 (1988).
[25] L. S. Zheng, C. M. Karner, P. J. Brucat, S. H. Yang, C. L. Pettiette, M. J. Craycraft, and R. E. Smalley, J. Chem. Phys. **85**, 1681 (1986).
[26] S. Krückeberg, L. Schweikhard, J. Ziegler, G. Dietrich, K. Lützenkirchen, and C. Walther, J. Chem. Phys. **114**, 2955 (2001).
[27] V. A. Spasov, T.-H. Lee, and K. M. Ervin, J. Chem. Phys. **112**, 1713 (2000).
[28] M. B. Knickelbein, J. Chem. Phys. **120**, 10450 (2004).
[29] D. Zajfman, O. Heber, L. Vejby-Christensen, I. Ben-Itzhak, M. Rappaport, R. Fishman, and M. Dahan, Phys. Rev. A **55**, R1577 (1997).
[30] H. Wollnik and M. Przewloka, Int. J. Mass Spectrom. Ion Processes **96**, 267 (1990).
[31] M. Lange, M. Froese, S. Menk, J. Varju, R. Bastert, K. Blaum, J. R. Crespo López-Urrutia, F. Fellenberger, M. Grieser, R. von Hahn, O. Heber, K.-U. Kühnel, F. Laux, D. A. Orlov, M. L. Rappaport, R. Repnow, C. D. Schröter, D. Schwalm, A. Shornikov, T. Sieber, Y. Toker, J. Ullrich, A. Wolf, and D. Zajfman, Rev. Sci. Instrum. **81**, 055105 (2010).
[32] A. Wucher and B. J. Garrison, J. Chem. Phys. **105**, 5999 (1996).
[33] A. Wucher, A. D. Bekkermanb, N. Kh. Dzhemilevb, S. V. Verkhoturovb, and I. V. Veryovkin, Nucl. Instrum. Methods B **140**, 311 (1998).
[34] J. U. Andersen, E. Bonderup, and K. Hansen, J. Phys. B: At. Mol. Opt. Phys. **35**, R1 (2002).
[35] K. Hansen, in *Statistical Physics of Nanoparticles in the Gas Phase*, Springer Series on Atomic, Optical, and Plasma Physics, Vol. 73 (Springer, Berlin, 2013), Chap. 5.
[36] M. F. Jarrold, in *Cluster of Atoms and Molecules I*, edited by H. Haberland (Springer, Berlin, 1994), p. 163.

[37] B. Kafle, O. Aviv, V. Chandrasekaran, O. Heber, M. L. Rappaport, H. Rubinstein, D. Schwalm, D. Strasser, and D. Zajfman, Phys. Rev. A **92**, 052503 (2015).
[38] T. Beyer and D. F. Swinehart, Commun. ACM **16**, 379 (1973).
[39] C. Walther, G. Dietrich, W. Dostal, K. Hansen, S. Krückeberg, K. Lützenkirchen, and L. Schweikhard, Phys. Rev. Lett. **83**, 3816 (1999).
[40] Y. Toker, O. Aviv, M. Eritt, M. L. Rappaport, O. Heber, D. Schwalm, and D. Zajfman, Phys. Rev. A **76**, 053201 (2007).
[41] S. Martin, J. Bernard, R. Brédy, B. Concina, C. Joblin, M. Ji, C. Ortega, and L. Chen, Phys. Rev. Lett. **110**, 063003 (2013).
[42] M. Goto, A. E. K. Sundén, H. Shiromaru, J. Matsumoto, H. Tanuma, T. Azuma, and K. Hansen, J. Chem. Phys. **139**, 054306 (2013).
[43] V. Chandrasekaran, B. Kafle, A. Prabhakaran, O. Heber, M. L. Rappaport, H. Rubinstein, D. Schwalm, Y. Toker, and D. Zajfman, J. Phys. Chem. Lett. **5**, 4078 (2014).
[44] K. Hansen and E. E. B. Campbell, Phys. Rev. E **58**, 5477 (1998).
[45] J. U. Andersen, H. Cederquist, J. S. Forster, B. A. Huber, P. Hvelplund, J. Jensen, B. Liu, B. Manil, L. Maunoury, S. Brøndsted Nielsen, U. V. Pedersen, H. T. Schmidt, S. Tomita, and H. Zettergren, Eur. Phys. J. D **25**, 139 (2003).
[46] K. Hansen, J. U. Andersen, P. Hvelplund, S. P. Møller, U. V. Pedersen, and V. V. Petrunin, Phys. Rev. Lett. **87**, 123401 (2001).
[47] J. U. Andersen, C. Brink, P. Hvelplund, M. O. Larsson, B. Bech Nielsen, and H. Shen, Phys. Rev. Lett. **77**, 3991 (1996).
[48] S. Menk, S. Das, K. Blaum, M. W. Froese, M. Lange, M. Mukherjee, R. Repnow, D. Schwalm, R. von Hahn, and A. Wolf, Phys. Rev. A **89**, 022502 (2014).
[49] M. W. Froese, K. Blaum, F. Fellenberger, M. Grieser, M. Lange, F. Laux, S. Menk, D. A. Orlov, R. Repnow, T. Sieber, Y. Toker, R. von Hahn, and A. Wolf, Phys. Rev. A **83**, 023202 (2011).
[50] M. H. Stockett, M. Kaminska, R. F. Nascimento, E. K. Anderson, M. Gatchell, K. Hansen, H. Zettergen, H. T. Schmidt, and H. Cederquist, J. Phys.: Conf. Ser. **635**, 072090 (2015).
[51] J. Fedor, K. Hansen, J. U. Andersen, and P. Hvelplund, Phys. Rev. Lett. **94**, 113201 (2005).
[52] M. Lange, M. W. Froese, S. Menk, D. Bing, F. Fellenberger, M. Grieser, F. Laux, D. A. Orlov, R. Repnow, T. Sieber, Y. Toker, R. von Hahn, A. Wolf, and K. Blaum, New J. Phys. **14**, 065007 (2012).
[53] G. Ito, T. Furukawa, H. Tanuma, J. Matsumoto, H. Shiromaru, T. Majima, M. Goto, T. Azuma, and K. Hansen, Phys. Rev. Lett. **112**, 183001 (2014).
[54] N. Kono, T. Furukawa, H. Tanuma, J. Matsumoto, H. Shiromaru, T. Azuma, K. Najafian, M. S. Pettersson, B. Dyneforse, and K. Hansen, Phys. Chem. Chem. Phys. **17**, 24732 (2015).
[55] M. Goto, J. Matsumoto, H. Shiromaru, Y. Achiba, T. Majima, H. Tanuma, and T. Azuma, Phys. Rev. A **87**, 033406 (2013).